




RESEARCH ARTICLE | AUGUST 25 2022

Straining of atomically thin WSe₂ crystals: Suppressing slippage by thermal annealing

Special Collection: [Advances in Multi-Scale Mechanical Characterization](#)

Wenshuai Hu; Yabin Wang; Kexin He; Xiaolong He; Yan Bai; Chenyang Liu; Nan Zhou; Haolin Wang; Peixian Li ; Xiaohua Ma; Yong Xie  

 Check for updates

J. Appl. Phys. 132, 085104 (2022)

<https://doi.org/10.1063/5.0096190>



Articles You May Be Interested In

Efficient modulation of MoS₂/WSe₂ interlayer excitons via uniaxial strain

Appl. Phys. Lett. (February 2022)

Strain engineering of quantum confinement in WSe₂ on nano-roughness glass substrates

Appl. Phys. Lett. (August 2022)

Characterization of quantum dot-like emitters in programmable arrays of nanowrinkles of 1L-WSe₂

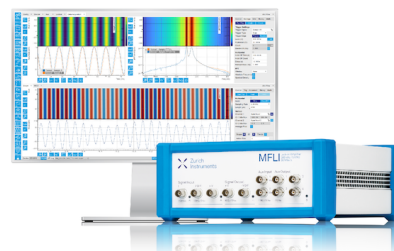
J. Appl. Phys. (July 2024)

Challenge us.

What are your needs for periodic signal detection?



[Find out more](#)



Straining of atomically thin WSe₂ crystals: Suppressing slippage by thermal annealing

Cite as: J. Appl. Phys. 132, 085104 (2022); doi: 10.1063/5.0096190

Submitted: 15 April 2022 · Accepted: 5 August 2022 ·

Published Online: 25 August 2022



Wenshuai Hu,¹ Yabin Wang,² Kexin He,¹ Xiaolong He,¹ Yan Bai,¹ Chenyang Liu,¹ Nan Zhou,¹ Haolin Wang,¹ Peixian Li,¹ Xiaohua Ma,¹ and Yong Xie^{1,a)}

AFFILIATIONS

¹Key Laboratory of Wide Band-Gap Semiconductor Technology, School of Advanced Materials and Nanotechnology, Xidian University, Xi'an 710071, China

²Department of Physics, Friedrich-Alexander-Universität Erlangen-Nürnberg (FAU), Staudtstraße 7, 91058 Erlangen, Germany

Note: This paper is part of the Special Topic on Advances in Multi-Scale Mechanical Characterization.

a) Author to whom correspondence should be addressed: yxie@xidian.edu.cn

ABSTRACT

The atomically thin two-dimensional (2D) transition-metal dichalcogenide (e.g., MoS₂) material can withstand large strains up to 11% to change its energy band structure, thereby further tuning its optical, electrical, and other physical properties. However, the slippage of 2D materials on substrate hampers the further strain tuning of the properties of 2D materials. Hereby, a facile three points approach combined with a dry transfer method that can apply uniaxial strain to two-dimensional materials is provided. The slippage of WSe₂ on polycarbonate (PC) substrate can be suppressed by thermally annealing WSe₂/PC in low pressure Ar atmosphere above 100 °C for 3 h. Straining cycle evolution experiments revealed that the thermal annealing of (1L) WSe₂ could suppress slippage from the surface of the PC. The spectral gauge factor of 1L WSe₂ is found to be around -60 meV/%. After thermal treatment, WSe₂/PC stacking can survive in DI water for at least 24 h without the degradation of the spectral gauge factor. Dome structures are formed after thermal treatments with the interplay of the viscoelasticity and surface tension of the PC and the 0.4% tensile strain on WSe₂, and the RMS roughness of WSe₂/PC increased from 820 to 1292 pm, indicating that there could be larger lateral friction force to suppress slippage following thermal annealing. Our findings enrich the strain engineering of 2D materials and their device applications.

Published under an exclusive license by AIP Publishing. <https://doi.org/10.1063/5.0096190>

I. INTRODUCTION

Changing the band structures of semiconductors by adjusting their atom distance through strain engineering could provide rich opportunities for altering their electrical, optical, and other physical properties. In the traditional semiconductor industry, strain can reduce the effective mass of carriers and hence increase carrier mobility.¹ Strain has recently become a usefully tuning knob for two-dimensional (2D) transition-metal dichalcogenide (TMDC) (e.g., MoS₂) materials by taking the advantage of the 11% elastic strain without breaking.² In order to affect the optical, electrical, magnetic, and optoelectrical properties of 2D materials, reversible strain was applied.^{3–9} Furthermore, at room temperature, atomically thin 2D transition-metal dichalcogenide (TMDC) exhibits exceptional exciton luminescence physics due to its direct bandgap and small environmental dielectric constant (air).^{4–6,10,11} Novel

phenomena such as exciton and dark exciton funneling could be revealed by strain with either AFM tip or nanostructured pillars by tuning with inhomogeneous (local) strain.^{10,12}

To regulate the strain in 2D materials, different approaches were used: bending with a flexible substrate, atomic force microscope (AFM) tip, buckling-induced delamination, piezoelectric substrate, micro-electro-mechanical systems (MEMS) actuator, pressurize, and bulging of 2D materials.^{12–17} Due to its simplicity, bending a flexible substrate with 2D materials on top has been the most popular and widely used methodology.¹⁷ Slippage, on the other hand, can occur often, and the spectral gauge factor (SGF, the ratio of relative change in photoluminescence excitonic peak, etc.) can be scattered with large variance.¹⁸ As a result, some changes are required to clamp the 2D materials either on top or on both ends of the 2D materials. To date, only a few attempts have been made to clamp 2D materials. For capping the surface of the monolayer MoSe₂, polydimethylsiloxane

25 October 2024 10:28:32

(PDMS) was chosen, and several straining cycles were measured to demonstrate the reproducibility of this method. A water-soluble poly (vinyl alcohol) (PVA) film was recently adopted to effectively encapsulate TMDC, resulting in a wide bandgap modulation of up to 300 meV and a large modulation spectral gauge factor of 136 meV/%.¹⁹ For the following scalable strain engineering applications of 2D materials and electronics, a study on employing different methods on TMDC is very desirable.

In the family of TMDC, tungsten diselenide (WSe_2) gain much attention because of its strong luminescence properties and the potential to be employed as quantum emitters.^{20,21} The band structures of bilayer WSe_2 change from indirect to direct bandgap when a strain larger than $\sim 0.625\%$ is applied.²² Strain-dependent energy shifts for the A, B, C, and D excitons of WSe_2 for uniaxial tensile strain in monolayer WSe_2 were probed by absorption measurements.²³ In uniaxially strained WSe_2 bilayers, the photoluminescence (PL) intensity was found to be enhanced by two orders of magnitude.²⁴ The spectral linewidth of the A exciton of WSe_2 decreases by a factor of 2 at room temperature due to the reduced exciton-phonon coupling.^{25,26}

However, the common issue of straining 2D materials is the diverse results given by different straining methods and groups. The scattered results of straining of 2D materials are governed primarily by three factors.¹⁸ First, the strain transfer between the substrate and the 2D materials, which is determined by the Young modules difference of the two materials.²⁷ Second, the friction force between the 2D materials and the substrate suppresses the relative slippage of materials with the substrate.^{28,29} Finally, the shape and size of the 2D material flake on the substrate also affect the strain transfer process.²⁷

Here, we use monolayer (1L) WSe_2 as a model material to investigate the influence of thermal annealing on the reversible strain engineering of 2D materials. We mainly focus on the changes of the bandgap PL spectra of WSe_2 under uniaxial strain with and without thermal annealing. More importantly, the roughness of the polycarbonate (PC) and WSe_2 on PC increased by 320 and 472 pm, respectively. The roughness increase enhances the lateral friction force and suppresses WSe_2 from slippage on PC. These experiments shine a light on the strain engineering of 2D materials and their applications in devices.

II. EXPERIMENTAL DETAILS

A. Dry transferring of WSe_2 onto PC

The bulk crystal was first exfoliated with scotch tape. The flake from the scotch tape was then further thinned down with blue Nitto tape (Nitto Denko Co., SPV 224P). A polydimethylsiloxane PDMS stamp (Gel-Fim[®] WF $\times 4$ 6.0 mil) was placed on top of the Nitto tape and pressed by a cotton swab. After PDMS was quickly detached from the Nitto tape and examined under an optical microscope. Flake as thin as a monolayer (1L) can be distinguished by transmittance or reflectance mode of the optical microscope (Nikon 150).

After discovering 1L WSe_2 with a suitable shape and size longer than $10\ \mu\text{m}$, we employ an all dry transfer method to transfer the flake onto PC. PDMS was cut and placed on a glass slide. After that, the glass slide was mounted on a three-dimensional micromanipulator. Then, the flake on PDMS was placed in the center of the PC, and the longest side was carefully aligned with the edge of the PC to maximize the strain applied on the flake.

B. Thermal annealing of WSe_2/PC stack in low pressure Ar atmosphere

The quartz tube is evacuated to 0.08 MPa with a vacuum pump before annealing, and then the Ar flow is switched on with a flow rate of 80 standard cubic centimeters per minute (SCCM). By adjusting the pumping rate, the pressure is stabilized at 0.08 MPa. The WSe_2/PC sample is heated to $100\ ^\circ\text{C}$ with a heating rate of $7.5\ ^\circ\text{C}/\text{min}$. After 3 h of heating, the heat was turned off and the furnace was cooled down naturally to room temperature.

C. Straining of atomically thin WSe_2

A facile device was designed to apply uniaxial strain to WSe_2 . The main idea of the device is to bend the material into an arch through the support in the center of the device [see Sect. S1 in the [supplementary material](#)]. Then, the arch height was calibrated through an optical microscope. We put the flexible substrate with two-dimensional materials on the support plate, search the flake under the microscope, and measure the height of the sample under the microscope (h_0). Then, we rotate the support screw in

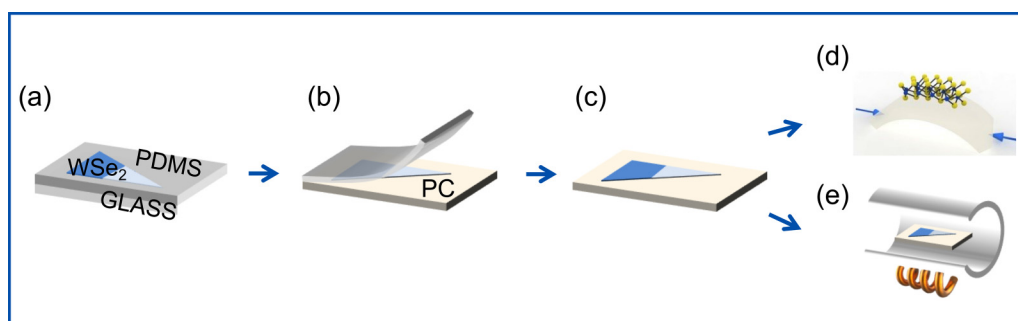


FIG. 1. Illustration of the dry transfer process of 2D semiconductors onto PC. (a) WSe_2 on PDMS on top of the glass side. (b) Dry transfer process of WSe_2 onto PC. (c) Removing PDMS and leaving WSe_2 on PC. (d) Bending the PC to strain WSe_2 on top. (e) Annealing WSe_2 to suppress the slippage of WSe_2 during bending.

25 October 2024 10:28:32

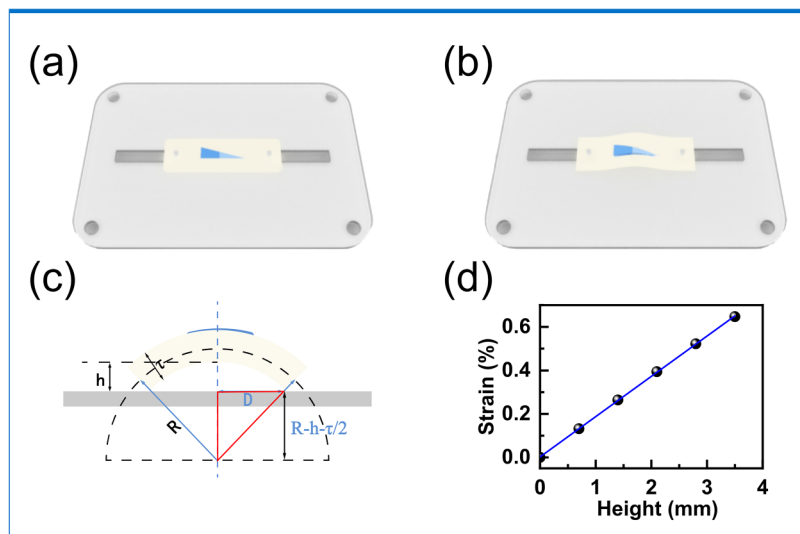
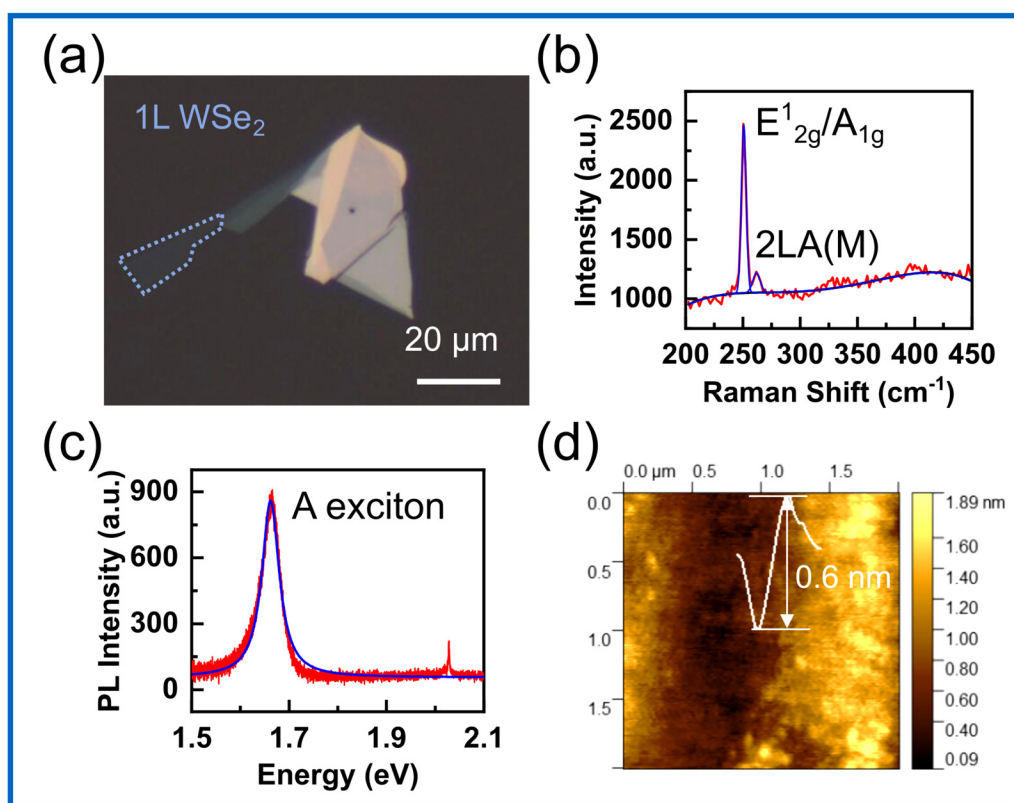


FIG. 2. Illustration of straining 2D materials using a facile three-point bending setup. (a) The homemade apparatus used to apply strain to the WSe_2 flake, which includes 2D materials (blue), a transparent substrate, two fixing screws (light gray), a screw (light gray), and the support plate (dark gray). (b) Side view of the strained device after bending. (c) Schematic diagram of the experimental setup with all parameters used for the strain calculation. (d) Uniaxial strain value as a function of the height applied on the screw.



25 October 2024 10:28:32

FIG. 3. Dry transferring 1L WSe_2 onto the PC substrate. (a) Optical micrograph of the 1L WSe_2 crystal transferred to PC by dry transfer method. The inset shows a cartoon of the geometry for 1L WSe_2 . (b) Raman spectra of the 1L WSe_2 crystal transfer onto the PC substrate. (c) Corresponding PL spectra of WSe_2 near 1.665 eV. (d) AFM topography of 1L WSe_2 , demonstrating the height of 1L WSe_2 and less contamination from PDMS.

the center (right under the flake) one turn, we refocus the flake under the microscope and record the height h_1 . After that, every time the screw is rotated one turn, the height is recorded. After rotating the screw for n turns, the height h_n is recorded. The average height \bar{h} of the change of the screw for one turn is calculated as follows:

$$\bar{h} = \frac{(h_n - h_{n-1}) + \dots + (h_2 - h_1) + (h_1 - h_0)}{n}. \quad (1)$$

D. Raman and PL spectroscopy

Raman and PL spectra are collected in backscattered geometry using a Renishaw inVia™ Raman spectrometer equipped with 1800 grooves/mm grating. The 532 nm green laser is focused through a 50× objective lens (NA 0.75). The laser power is kept below 0.1 mW to avoid laser heating effects and photo doping.

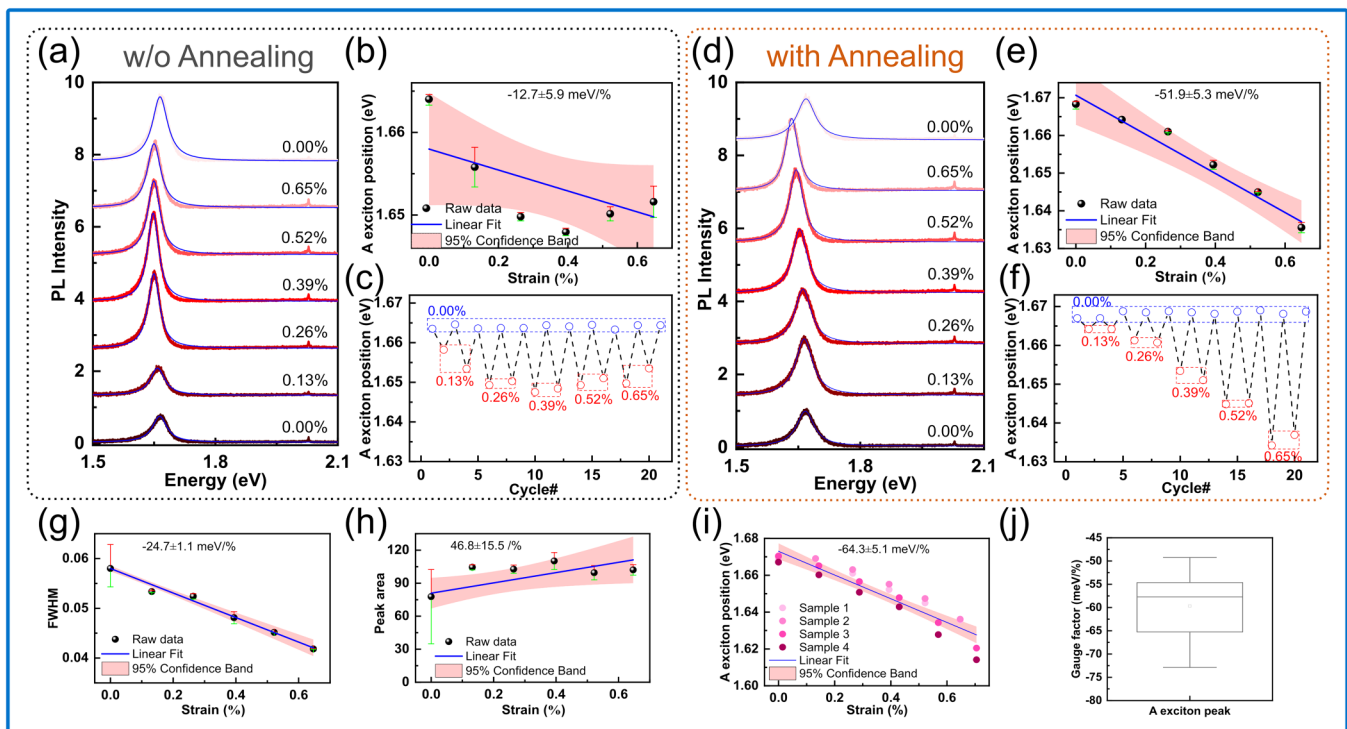
III. RESULTS AND DISCUSSIONS

To get high quality materials, we use a sophisticated, developed, all dry transfer method to transfer exfoliated WSe₂ onto PC

as shown in the method section of the literature.³⁰ After transferred on PC, the atomically thin WSe₂ can be either directly used for straining [Fig. 1(c)] or annealed first [Fig. 1(e)] and then applying uniaxial strain on the PC to transfer the strain on WSe₂.

A facile three points bending setup was utilized to bend the PC, thus straining the 2D materials. The device is composed of a support plate, two fixing screws, and a screw located in the center of the support plate, as shown in Figs. 2(a) and 2(b). The strain is applied to the substrate and is mainly controlled by the central screw of the supporting plate. The material is dry transferred to the center of the target substrate. The screw under pressure is rotated to lift the center of the substrate, and the substrate is bent into an arch. The front view of the device after bending is shown in Fig. 2(b). Figure 2(c) is a schematic diagram of the experimental device with all the parameters used for strain calculation. Every time the screw rotates, the center of the substrate will rise by \bar{h} (0.7 mm) (measured under the microscope), so when the screw is rotated n turns, the height h of the sample changes

$$h = n\bar{h}, \quad (2)$$



25 October 2024 10:28:32

FIG. 4. Straining of 1L WSe₂ without and with thermal annealing of the PC substrate. (a) PL spectra of 1L WSe₂ without thermal annealing by applying different strains. (b) The strain dependence A exciton with peak positions extracted from (a), the spectral gauge factor is calculated to be -12.7 ± 5.9 meV/%. (c) PL spectra of 1L WSe₂ with strain cycle evolution. (d) PL spectra of 1L WSe₂ with thermal annealing by applying different strains. (e) The strain dependence A exciton with peak positions extracted from (d), the spectral gauge factor is calculated to be -51.9 ± 5.3 meV/%. (f) PL spectra of 1L WSe₂ with strain cycle evolution. (g) The dependence of full width at half maximum extracted with strain from the fitting curves of (d). (h) The dependence of peak area extracted with strain from the fitting curves of (d). (i) Summary of the A exciton position change with strain for four different samples. (j) Corresponding box statistics of spectral gauge factors extracted from (i).

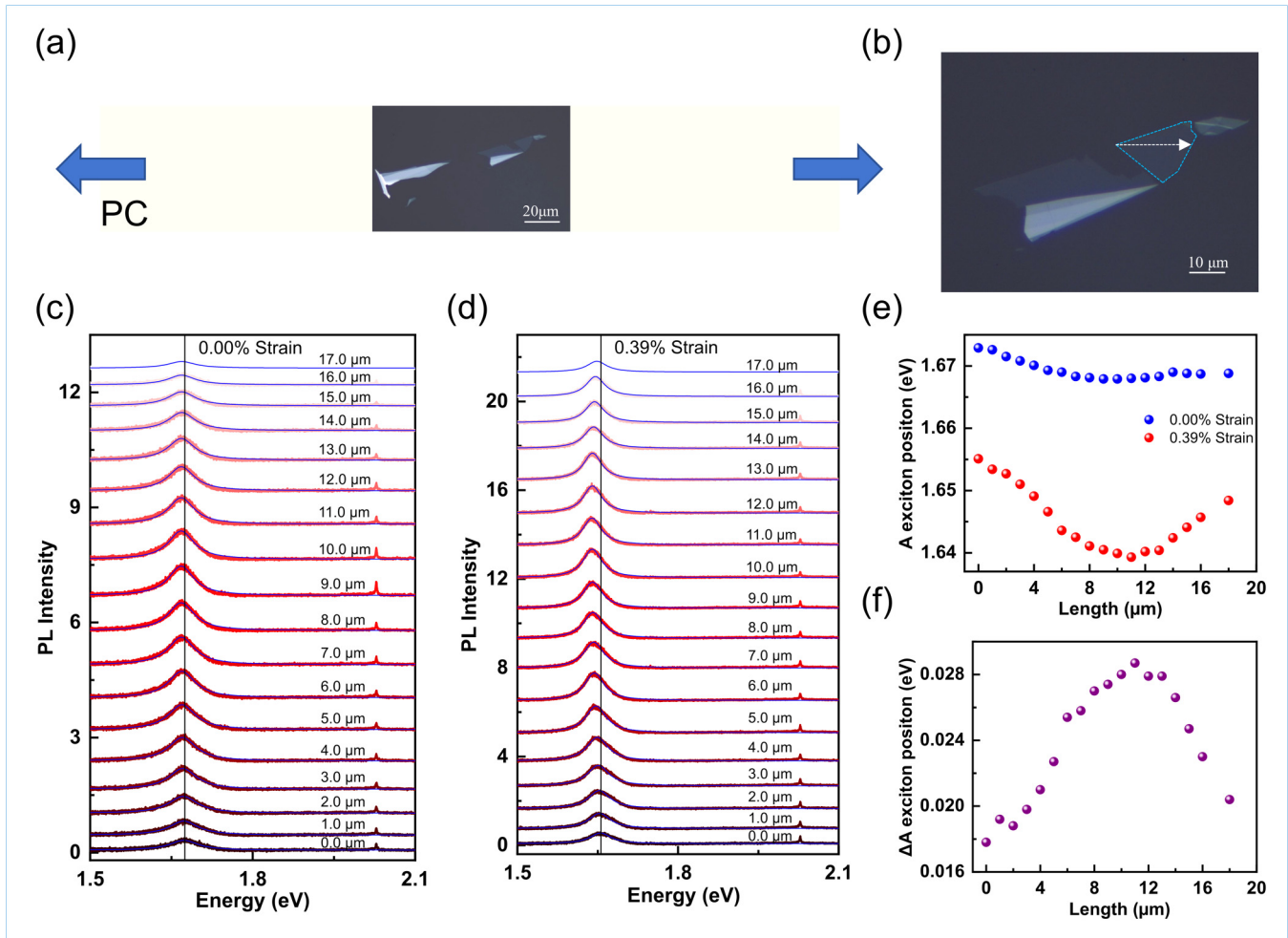


FIG. 5. Straining of 1L WSe₂ with Raman line scan after thermal annealing. (a) The position of 1L WSe₂ on the PC. (b) Optical micrograph of the 1L WSe₂ crystal. (c) PL spectra of 1L WSe₂ with 0 external strain with line scan. (d) PL spectra of 1L WSe₂ under 0.39% strain with line scan. (e) A exciton with peak positions extracted from (c) and (d). (f) A exciton peak positions differ between 0 external strain and 0.39% strain.

then the radius R can be calculated as [using the red triangle in Fig. 2(c)]

$$D^2 + \left(R - h - \frac{\tau}{2}\right)^2 = \left(R - \frac{\tau}{2}\right)^2. \quad (3)$$

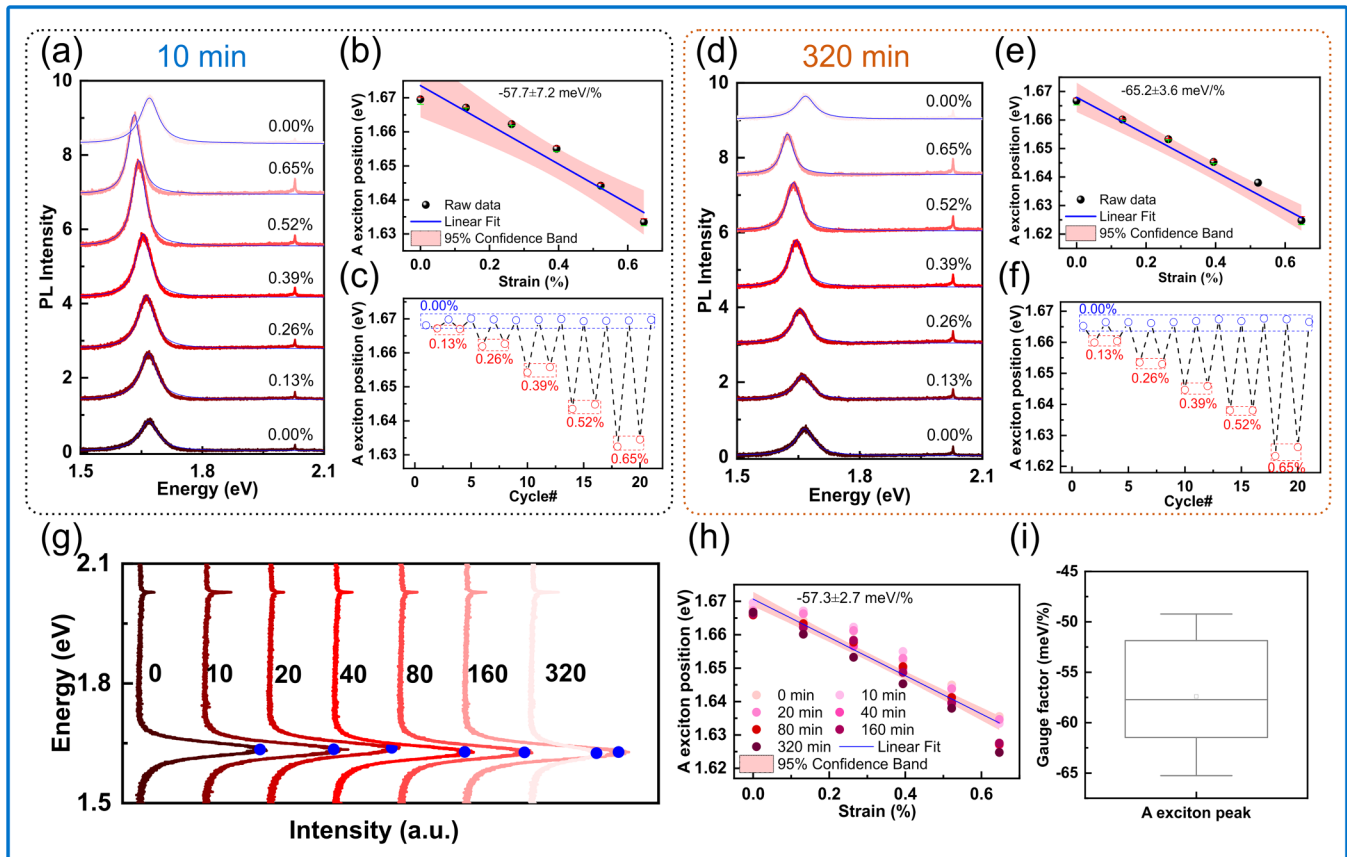
From this, the strain applied to the material can be calculated as²³

$$\epsilon = \frac{\tau}{2R}, \quad (4)$$

where τ is the thickness of the substrate. Here, we use a flexible substrate PC with a thickness of 1 mm, D is the half of the distance between the two fixing screws (23 mm), and R is the radius of

curvature of the material after bending. Figure 2(d) is uniaxial strain as a function of height h . The greater the h , the uniaxial strain increases significantly. The strain increases linearly with h .

To ensure that the applied strain is effectively transferred from the substrate to the material, the effective transfer of the material is essential. The optical micrograph of 1L WSe₂ transferred onto a PC substrate is shown in Fig. 3(a). The 1L part of WSe₂ is marked by blue dotted lines. Raman and PL spectra were used to characterize 1L WSe₂. The Lorentz function is used to fit the data, and for Raman, Gaussian function fitting is used for the fitting of PL spectra. Only one Raman peak was observed at 250 cm⁻¹, which is degenerated A_{1g} and E_{2g}¹, with the A_{1g} mode being out-of-plane vibration and the E_{2g}¹ mode being in-plane vibration. The degeneration of A_{1g} and E_{2g}¹ confirms the monolayer nature of the flake.³¹



25 October 2024 10:28:32

FIG. 6. Straining of 1L WSe₂ without and with thermal annealing of the PC substrate. (a) PL spectra of 1L WSe₂ without thermal annealing by applying different strains. (b) The strain dependence A exciton with peak positions extracted from (a), the slope of spectral gauge factor is calculated to be -57.7 ± 7.2 meV/%. (c) PL spectra of 1L WSe₂ with strain cycle evolution. (d) PL spectra of 1L WSe₂ with thermal annealing by applying different strains. (e) The strain dependence A exciton with peak positions extracted from (d), the slope of spectral gauge factor is calculated with a slope of -65.2 ± 3.6 meV/%. (f) PL spectra of 1L WSe₂ with strain cycle evolution. (g) The PL spectra of 1L WSe₂ after dipping in DI water with different times: from 0 to 320 min. (h) Summary of the uniaxial strain on 1L WSe₂ after dipping in DI water at different times. (i) Corresponding statistical information of the spectral gauge factors at different dipping times.

The peak located at 262 cm^{-1} is the 2LA(M) mode, which can be attributed to the second-order Raman mode due to LA phonons at the M point in the Brillouin zone. Photoluminescence of WSe₂ shows only one dominant peak at 1.665 eV, which arises from A exciton recombination.³² Atomic force microscope (AFM) topography was also measured on the flake and a height of 0.6 nm was obtained, further proving the atomic thinness of WSe₂ on PC and less contamination from the dry transfer process.

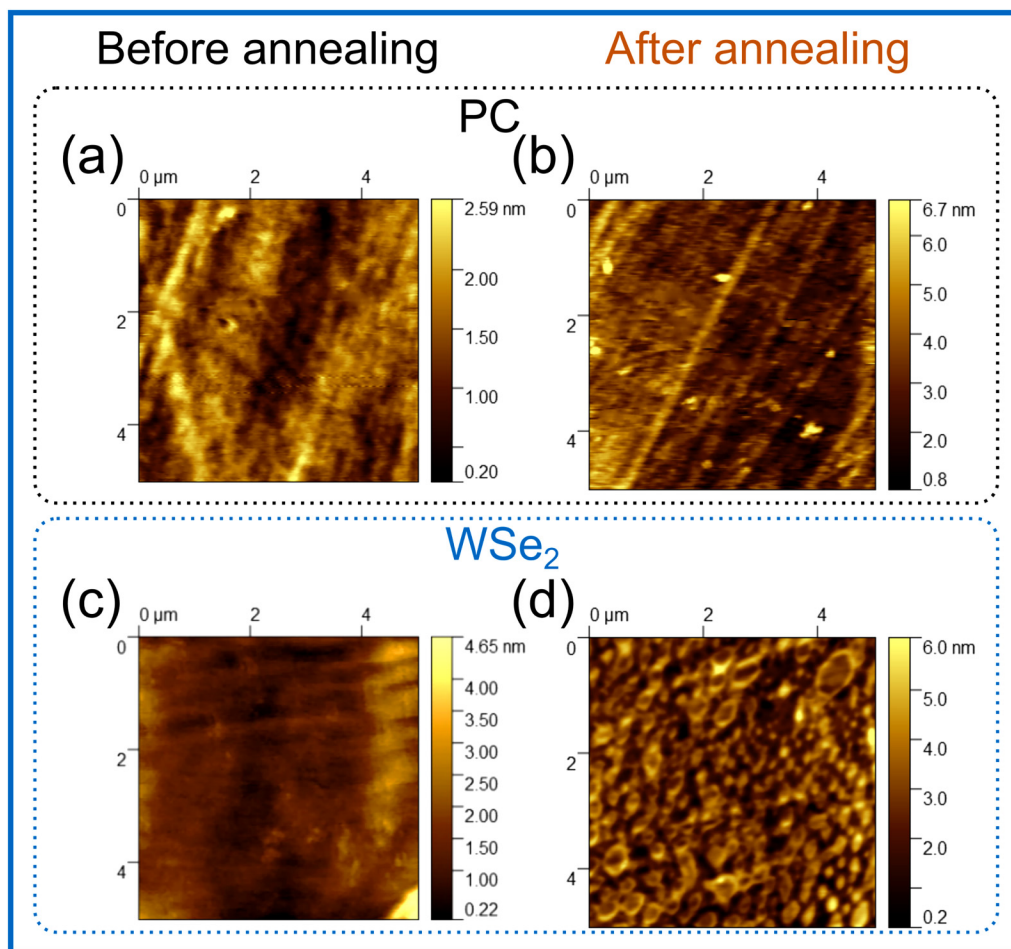
After transferring onto PC, the straining test can be performed on the 1L WSe₂. PL spectra of the 1L WSe₂ after applying uniaxial strain to the PC substrate are shown in Fig. 4(a). The A exciton peak has redshifts with strain increases up to 0.65% under tensile strain. With the strain decreasing from 0.65% to 0%, the A exciton peak of monolayer WSe₂ shifts back to 1.665 eV. The A exciton peak does not shift to lower energy with increased strain levels in the strain cycle evolution test in Fig. 4(c), which is a common indication of relative slippage between WSe₂ and the PC substrate.¹⁹

To solve the slippage problem, a thermal annealing process in low pressure Ar atmosphere was performed on the WSe₂/PC stack, the main corresponding results are shown in Figs. 4(d)–4(f). Figures 5(d) and 5(e) show the evolution of the PL spectra of 1L WSe₂ with different uniaxial strains. The A exciton peak redshifted from 1.668 eV at zero external strain to 1.636 eV at 0.65% tensile strain. The A exciton peak of 1L WSe₂ changes with strain linearly after the thermal annealing under low pressure Ar atmosphere.

Here, to quantitatively qualify the relationship of the strain, we define the spectral shift per % of uniaxial strain as our strain spectral gauge factor (SGF),³⁵

$$\text{SGF} = \frac{\Delta E}{\varepsilon}, \quad (5)$$

where the ΔE is the energy shift during the PL measurements and ε is the corresponding strain in the range of PL measurements.



25 October 2024 10:28:32

FIG. 7. AFM micrograph of PC and 1L WSe₂ without and with thermal annealing. AFM topography of PC (a) without and (b) with thermal annealing. AFM topography of WSe₂ on PC (c) without and (d) with thermal annealing.

The spectral strain spectral gauge factor can be calculated to be the slope of Fig. 4(e). A spectral gauge factor of -51.9 ± 5.3 meV/% for the A exciton is obtained. To verify the reproducibility of the strain, PL spectra of 1L WSe₂ with strain cycle evolution were shown in Fig. 4(f). We can see that the A exciton peak shifts back to zero external strain peak after the withdrawal of the strain of PC, further proving the effectiveness of the thermal annealing under low pressure Ar atmosphere.

At room temperature, the width of A exciton is governed by the exciton–phonon interaction. Therefore, an asymmetric line shape of A exciton peak could be resolved from PL or reflection measurement.²⁶ Intervalley scattering processes dominate the A exciton luminescence of 1L WSe₂. The A exciton in 1L WSe₂ is efficiently scattered by phonon without external strain, thus having a broad A exciton peak full width at half maximum (FWHM). The band structure changes with uniaxial strain, and the intervalley phonon scattering process is reduced, thus leading to the narrower

FWHM of A exciton.²⁶ The FWHM of A exciton decreased from 58 meV without external strain to 42 meV at 0.65% strain [as shown in Fig. 4(g)] with a slope of -25 meV/%, which is much significantly greater than the previous values.²⁶ We were able to repeatedly reach similar tuning behaviors by performing the thermal annealing on different 1L WSe₂ samples on PC [Fig. 4(i)]. The detail can be found in the [supplementary material](#), Table S1 and Figs. S3 and S4. Figures 4(j) and 4(h) show the summary of the four different samples with changing strain, where the average spectral gauge factor is -57.3 ± 3.6 meV.

In order to obtain more information along the tensile force direction of the flake, a PL line scan was carried out along the direction of tensile force as shown in Figs. 5(a) and 5(b).³⁴ It can be seen that the PL spectra from the center part of the flake has a redshift, indicating that the center part of the flake experiences a tensile strain compared with the edge part [Figs. 5(c) and 5(d)]. Therefore, we typically measure the center part of the flake

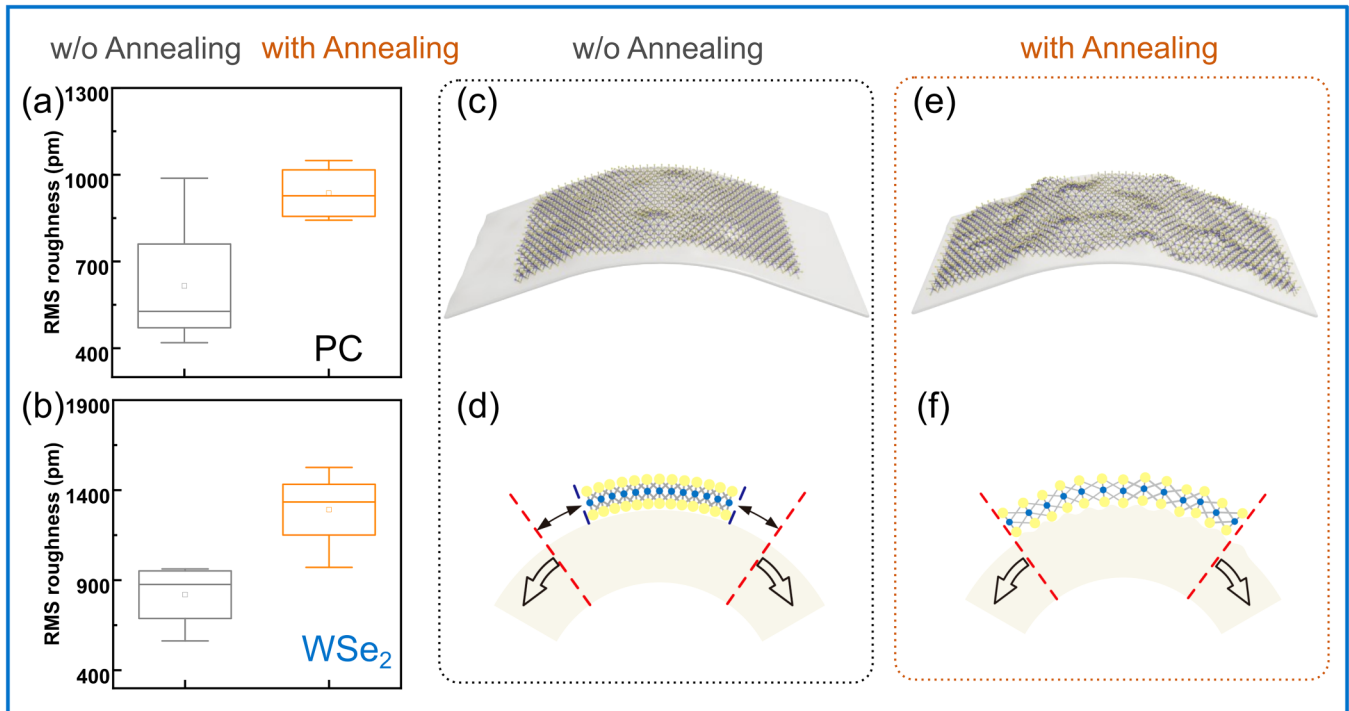


FIG. 8. Mechanism of suppression of slippage by thermal annealing. AFM roughness of bare PC (a) and WSe₂ on PC (b) without and with annealing. Schematic morphology changes related to the slippage without thermal annealing [(c) and (d)] and with thermal annealing [(e) and (f)]. The red dashed line marks the ideal position without slippage, and the blue dashed line marks the actual position of the WSe₂ edge with slippage.

away from the edge to ensure the full strain transfer of the flake. Figure 5(e) shows the extracted peak positions from PL spectra in Figs. 5(c) and 5(d).

To evaluate the reproducibility of the straining and the robustness of the adhesion force of WSe₂ on PC after annealing, we dipped the WSe₂/PC stack into DI water and then dry the samples before performing the PL measurement. Figure 6(a) shows the PL spectra of a 1L of WSe₂ transferred onto a PC substrate after dipping in DI water from 10 to 320 min. All the results show the reversible behavior with strain up to 320 min dipping in DI water. Please note that there is no slippage by dipping in DI water for at least 24 h (the results are included in the supplementary material, Figs. S7 and S8). The spectral gauge factor obtained from the straining experiments shows no evidence of slippage, which confirms the atomically impermeable interface of WSe₂ and PC. This fascinating phenomenon could be very useful for the design and realization of nanoelectromechanical systems (NEMSs)^{15,16} or sensing in liquid using 2D materials.³⁵

AFM topography for PC and WSe₂ on PC before and after thermal annealing was compared to gain a better understanding of the mechanism of slippage. As shown in Fig. 7, the surface roughness of PC increased from 419 to 985 pm, while the surface roughness of WSe₂ on PC increased from 563 to 972 pm. In addition, the morphology of PC and WSe₂ changed dramatically after thermal annealing. For WSe₂ on PC after annealing, many particle shape

domes were observed [Fig. 7(d)] in comparison to PC and WSe₂ before annealing. Moreover, four different PC and WSe₂ flakes on PC were chosen to verify this finding, as shown in Figs. 8(a) and 8(b). The surface roughness of all four samples increases in the same way after thermal annealing. The sliding friction with the roughness of substrate for atomically thin materials (e.g., MoS₂) is quantitatively analyzed.³⁶ The slide friction of MoS₂ could be reduced by five times by using a flatter h-BN surface. In our case, the lateral friction force between WSe₂ and PC could be increased by increasing the roughness of WSe₂. Eventually, the lateral friction force could balance the force of the substrate and suppress the slippage as demonstrated in Figs. 8(e) and 8(f).

With heating up to 100 °C, there is tensile strain generated due to the thermal expansion coefficient mismatch of WSe₂ ($\alpha_{\text{WSe}_2} = 9.5 \times 10^{-6} \text{ K}^{-1}$) and PC ($\alpha_{\text{PC}} = 68 \times 10^{-6} \text{ K}^{-1}$) during the thermal annealing process. The strain between the PC substrate and WSe₂ can be calculated as follows:³⁷

$$\epsilon(T_A) = \int_{25^\circ\text{C}}^{T_A} \alpha_{\text{WSe}_2}(T) dT - \int_{25^\circ\text{C}}^{T_A} \alpha_{\text{PC}}(T) dT. \quad (6)$$

At the annealing temperature of 100 °C (T_A), WSe₂ is under 0.4% of the biaxial tensile strain. Although PC has a glass transition temperature of 145–150 °C, PC could be soft at the temperature of

100 °C. Therefore, dome-shaped structures formed because of the interplay of the viscoelasticity and surface tension of the PC and the tensile strain of WSe₂. Finally, the overall roughness increased after thermal annealing. Moreover, the tensile strain is also preserved partially after the thermal annealing, as shown in Fig. 5(e).

IV. CONCLUSIONS

In conclusion, here a facile straining setup and corresponding calibration were developed. 1L WSe₂ was employed as a model material to test the validity of the slippage and related suppression. We found that annealing at 100 °C for 3 h in the tube furnace can substantially increase the surface roughness and hence the lateral friction force, leading to the reversible straining process. We have demonstrated that a reproducible tensile strain of up to 0.65% can be obtained. A exciton with increased uniaxial strain with slopes of around -60 meV/% could be achieved. The WSe₂/PC stack can sustain without any indication of slippage by dipping in DI water for at least 24 h. These findings will pave the way for straining 2D materials and related processes with NEMSS devices. We noticed that PC is also used for the clean transferring of 2D materials.^{38,39} Based on our experiments, we can also anticipate that the annealing temperature during the transfer could be critical for the pickup of the 2D materials.

SUPPLEMENTARY MATERIAL

See the [supplementary material](#) for the straining setup and datasets of the slippage and related suppression of 1L WSe₂.

ACKNOWLEDGMENTS

Financial support from the National Natural Science Foundation of China (NSFC) Grant (Nos. 62011530438, 61704129, and 21901195) is acknowledged. This work was partially supported by the Key Research and Development Program of Shaanxi (Program No. 2021KW-02), Natural Science Foundation of Shaanxi Province (Grant No. 2019JQ-155), and Fundamental Research Funds for the Central Universities (Nos. JB211409 and 20103206819) and the fund of the State Key Laboratory of Solidification Processing in Northwestern Polytechnical University (Grant No. SKLSP201612). Special thanks are due to Andres Castellanos-Gomez and Klaus Thonke for their continuous encouragement and support.

AUTHOR DECLARATIONS

Conflict of Interest

The authors have no conflicts to disclose.

Author Contributions

W.H. and Y.W. contributed equally to this work.

Wenshuai Hu: Investigation (lead); Visualization (lead). **Yabin Wang:** Writing – review & editing (equal). **Kexin He:** Investigation (equal); Visualization (equal). **Xiaolong He:** Investigation (equal); Visualization (equal). **Yan Bai:** Investigation (equal). **Chenyang Liu:** Investigation (equal). **Nan Zhou:** Investigation (equal). **Haolin Wang:** Investigation (equal).

Peixian Li: Resources (equal). **Xiaohua Ma:** Resources (equal). **Yong Xie:** Conceptualization (lead); Data curation (lead); Formal analysis (lead); Funding acquisition (lead); Investigation (equal); Methodology (lead); Project administration (lead); Resources (lead); Software (equal); Supervision (lead); Validation (lead); Visualization (equal); Writing – original draft (lead); Writing – review & editing (equal).

DATA AVAILABILITY

The data that support the findings of this study are available from the corresponding author upon reasonable request.

REFERENCES

- ¹M. Chu, Y. Sun, U. Aghoram, and S. Thompson, *Annu. Rev. Mater. Res.* **39**, 203–229 (2009).
- ²S. Bertolazzi, J. Brivio, and A. Kis, *ACS Nano* **5**(12), 9703–9709 (2011).
- ³P. Gant, P. Huang, D. Pérez de Lara, D. Guo, R. Frisenda, and A. Castellanos-Gomez, *Mater. Today* **27**, 8–13 (2019).
- ⁴H. Kim, S. Z. Uddin, N. Higashitarumizu, E. Rabani, and A. Javey, *Science* **373**, 6553 (2021).
- ⁵H. Kim, S. Z. Uddin, D. Lien, M. Yeh, N. S. Azar, S. Balendhran, T. Kim, N. Gupta, Y. Rho, C. P. Grigoropoulos, K. B. Crozier, and A. Javey, *Nature* **596**, 7871 (2021).
- ⁶J. Cenker, S. Sivakumar, K. Xie, A. Miller, P. Thijssen, Z. Liu, A. Dismukes, J. Fonseca, E. Anderson, X. Zhu, X. Roy, D. Xiao, J.-H. Chu, T. Cao, and X. Xu, *Nat. Nanotechnol.* **17**, 256–261 (2022).
- ⁷Z. Dai, L. Liu, and Z. Zhang, *Adv. Mater.* **31**, 45 (2019).
- ⁸Z. Dai, N. Lu, K. M. Liechti, and R. Huang, *Curr. Opin. Solid State Mater. Sci.* **24**, 4 (2020).
- ⁹Y. Zhou, S. Zhou, P. Ying, Q. Zhao, Y. Xie, M. Gong, P. Jiang, H. Cai, B. Chen, S. Tongay, J. Zhang, W. Jie, T. Wang, P. Tan, D. Liu, and M. Kuball, *J. Phys. Chem. Lett.* **13**(17), 3831–3839 (2022).
- ¹⁰M. G. Harats, J. N. Kirchhof, M. Qiao, K. Greben, and K. I. Bolotin, *Nat. Photonics* **14**, 324–329 (2020).
- ¹¹R. Frisenda and A. Castellanos-Gomez, *Nat. Photonics* **14**, 269–270 (2020).
- ¹²R. Rafael, A. Castellanos-Gomez, C. Emmanuele, and G. Francisco, *J. Phys.: Condens. Matter* **27**, 313201 (2015).
- ¹³K. Cao, S. Feng, Y. Han, L. Gao, T. Hue Ly, Z. Xu, and Y. Lu, *Nat. Commun.* **11**, 284 (2020).
- ¹⁴J. Quereda and A. Castellanos-Gomez, *Nat. Photonics* **16**(3), 179–180 (2022).
- ¹⁵Y. Xie, J. Lee, Y. Wang, and P. X.-L. Feng, *Adv. Mater. Technol.* **6**, 2000794 (2021).
- ¹⁶Y. Xie, J. Lee, H. Jia, and P. X.-L. Feng, “Frequency tuning of two-dimensional nanoelectromechanical resonators via comb-drive MEMS actuators,” in *International Conference on Solid-State Sensors, Actuators and Microsystems & Eurosensors XXXIII (Transducers & Eurosensors XXXIII)* (IEEE, 2019).
- ¹⁷J. O. Island, A. Kuc, E. H. Diependaal, R. Bratschitsch, H. S. J. van der Zant, T. Heine, and A. Castellanos-Gomez, *Nanoscale* **8**, 2589–2593 (2016).
- ¹⁸F. Carrascoso, H. Li, R. Frisenda, and A. Castellanos-Gomez, *Nano Res.* **14**, 1698–1703 (2021).
- ¹⁹Z. Li, Y. Lv, L. Ren, J. Li, L. Kong, Y. Zeng, Q. Tao, R. Wu, H. Ma, B. Zhao, D. Wang, W. Dang, K. Chen, L. Liao, X. Duan, and Y. Liu, *Nat. Commun.* **11**, 1151 (2020).
- ²⁰C. Palacios-Berraquero, D. M. Kara, A. R. P. Montblanch, M. Barbone, P. Latawiec, D. Yoon, A. K. Ott, M. Loncar, A. C. Ferrari, and M. Atatüre, *Nat. Commun.* **8**, 15093–15099 (2017).
- ²¹S. Kumar, A. Kaczmarczyk, and B. D. Gerardot, *Nano Lett.* **15**, 3312 (2015).
- ²²S. B. Desai, G. Seol, J. S. Kang, H. Fang, C. Battaglia, R. Kapadia, J. W. Ager, J. Guo, and A. Javey, *Nano Lett.* **14**, 4592–4597 (2014).

- ²³R. Schmidt, I. Niehues, R. Schneider, M. Drüppel, T. Deilmann, M. Rohlfing, S. M. de Vasconcellos, A. Castellanos-Gomez, and R. Bratschitsch, *2D Mater.* **3**, 021011 (2016).
- ²⁴W. Wu, J. Wang, P. Ercius, N. C. Wright, D. M. Leppert-Simenauer, R. A. Burke, M. Dubey, A. M. Dogare, and M. T. Pettes, *Nano Lett.* **18**, 2351–2357 (2018).
- ²⁵O. B. Aslan, M. Deng, M. L. Brongersma, and T. F. Heinz, *Phys. Rev. B* **101**, 115305 (2020).
- ²⁶I. Niehues, R. Schmidt, M. Drüppel, P. Maruhn, D. Christiansen, M. Selig, G. Berghäuser, D. Wigger, R. Schneider, L. Braasch, R. Koch, A. Castellanos-Gomez, T. Kuhn, A. Knorr, E. Malic, M. Rohlfing, S. M. de Vasconcellos, and R. Bratschitsch, *Nano Lett.* **18**, 1751–1757 (2018).
- ²⁷Z. Liu, M. Amani, S. Najmaei, Q. Xu, X. Zou, W. Zhou, T. Yu, C. Qiu, A. G. Birdwell, F. J. Crowne, R. Vajtai, B. I. Yakobson, Z. Xia, M. Dubey, P. M. Ajayan, and J. Lou, *Nat. Commun.* **5**, 5246 (2014).
- ²⁸Z. Dai and N. Lu, *J. Mech. Phys. Solids* **149**, 104320 (2021).
- ²⁹Z. Dai, D. A. Sanchez, C. J. Brennan, and N. Lu, *J. Mech. Phys. Solids* **137**, 103843 (2020).
- ³⁰A. Castellanos-Gomez, M. Buscema, R. Molenaar, V. Singh, L. Janssen, H. S. J. van der Zant, and G. A. Steele, *2D Mater.* **1**, 011002 (2014).
- ³¹W. Zhao, Z. Ghorannevis, K. K. Amara, J. R. Pang, M. Toh, X. Zhang, C. Kloc, P. H. Tan, and G. Eda, *Nanoscale* **5**, 9677–9683 (2013).
- ³²P. Tonndorf, R. Schmidt, P. Böttger, X. Zhang, J. Börner, A. Liebig, M. Albrecht, C. Kloc, O. Gordan, D. R. T. Zahn, S. Michaelis de Vasconcellos, and R. Bratschitsch, *Opt. Express* **21**, 4908–4916 (2013).
- ³³R. Frisenda, M. Drüppel, R. Schmidt, S. Michaelis de Vasconcellos, D. Perez de Lara, R. Bratschitsch, M. Rohlfing, and A. Castellanos-Gomez, *NPJ 2D Mater. Appl.* **1**, 10 (2017).
- ³⁴Z. Dai, G. Wang, L. Liu, Y. Hou, Y. Wei, and Z. Zhang, *Compos. Sci. Technol.* **136**, 1–9 (2016).
- ³⁵E. Gil-Santos, J. J. Ruz, O. Malvar, I. Favero, A. Lemaître, P. M. Kosaka, S. García-López, M. Calleja, and J. Tamayo, *Nat. Nanotechnol.* **15**, 469–474 (2020).
- ³⁶J. Quereda, A. Castellanos-Gomez, N. Agraït, and G. Rubio-Bollinger, *Appl. Phys. Lett.* **105**, 053111 (2014).
- ³⁷G. H. Ahn, M. Amani, H. Rasool, D. H. Lien, J. P. Mastandrea, J. W. Ager III, M. Dubey, D. C. Chrzan, A. M. Minor, and A. Javey, *Nat. Commun.* **8**, 608 (2017).
- ³⁸Y.-C. Lin, C. Jin, J.-C. Lee, S.-F. Jen, K. Suenaga, and P.-W. Chiu, *ACS Nano* **5**, 2362–2368 (2011).
- ³⁹R. Frisenda, E. Navarro-Moratalla, P. Gant, D. Pérez De Lara, P. Jarillo-Herrero, R. V. Gorbachev, and A. Castellanos-Gomez, *Chem. Soc. Rev.* **47**, 53–68 (2018).